Single-step implementation of a hybrid controlled-NOT gate with one superconducting qubit simultaneously controlling multiple target cat-state qubits

Qi-Ping Su[1], Yu Zhang[2], and Chui-Ping Yang[1,3*]

[1]*Department of Physics, Hangzhou Normal University, Hangzhou 311121, China*

[2]*School of Physics, Nanjing University, Nanjing 210093, China and*

[3]*Quantum Information Research Center, Shangrao Normal University, Shangrao 334001, China*
(Dated: August 30, 2022)

Hybrid quantum gates have recently drawn considerable attention. They play significant roles in connecting quantum information processors with qubits of different encoding and have important applications in the transmission of quantum states between a quantum processor and a quantum memory. In this work, we propose a single-step implementation of a multi-target-qubit controlled-NOT gate with one superconducting (SC) qubit simultaneously controlling n target cat-state qubits. In this proposal, the gate is implemented with n microwave cavities coupled to a three-level SC qutrit. The two logic states of the control SC qubit are represented by the two lowest levels of the qutrit, while the two logic states of each target cat-state qubit are represented by two quasi-orthogonal cat states of a microwave cavity. This proposal operates essentially through the dispersive coupling of each cavity with the qutrit. The gate realization is quite simple because it requires only a single-step operation. There is no need of applying a classical pulse or performing a measurement. The gate operation time is independent of the number of target qubits, thus it does not increase as the number of target qubits increases. Moreover, because the third higher energy level of the qutrit is not occupied during the gate operation, decoherence from the qutrit is greatly suppressed. As an application of this hybrid multi-target-qubit gate, we further discuss the generation of a hybrid Greenberger-Horne-Zeilinger (GHZ) entangled state of SC qubits and cat-state qubits. As an example, we numerically analyze the experimental feasibility of generating a hybrid GHZ state of one SC qubit and three cat-state qubits within present circuit QED technology. This proposal is quite general and can be extended to implement a hybrid controlled-NOT gate with one matter qubit (of different type) simultaneously controlling multiple target cat-state qubits in a wide range of physical systems, such as multiple microwave or optical cavities coupled to a three-level natural or artificial atom.

PACS numbers: 03.67.Bg, 42.50.Dv, 85.25.Cp

I. INTRODUCTION AND MOTIVATION

Circuit quantum electrodynamics (QED), composed of microwave cavities and superconducting (SC) qubits, has appeared as one of the most promising candidates for quantum information processing (QIP) [1-7]. SC qubits (e.g., flux qubits, transmon qubits, Xmon qubits, fluxonium qubits, etc.) can be flexibly and easily fabricated with microwave cavities, by using modern integrated circuit technology. After more than 20 years of development, the coherence time of SC qubits has leaped from the initial order of nanoseconds to the order of hundreds of microseconds [8,9] or even over one millisecond [10,11]. Due to their improved long coherence time and energy-level spacings being rapidly adjustable [12-14], SC qubits are often used as the basic processing units for solid-state QIP. So far, quantum gates with 2 SC qubits [15-27], 3 SC qubits [28,29], and 4 SC qubits [29] have been experimentally demonstrated. In addition, quantum entangled states of 2-6 SC qubits [12,18,30,31], 10-12 SC qubits [19,32,33], and 18-20 SC qubits [34,35] have been created in experiments.

On the other hand, one-dimensional (1D) microwave resonators of high quality factor $Q \gtrsim 10^6$ [36-41] and three-dimensional (3D) microwave cavities with high quality factor $Q \gtrsim 3.5 \times 10^7$ [42-44] have been reported in experiments. Owing to the experimental demonstration of high-quality factors, microwave cavities or resonators contain microwave photons with a lifetime comparable to that of SC qubits [45]. Quantum state engineering and QIP using microwave fields and photons have recently drawn much attention. In particular, there is an increasing interest in QIP with cat-state qubits (i.e., qubits encoded with cat states) due to their enhanced lifetime with quantum error correction (QEC) [46]. Various proposals have been presented for implementing a universal set of single- and two-qubit gates
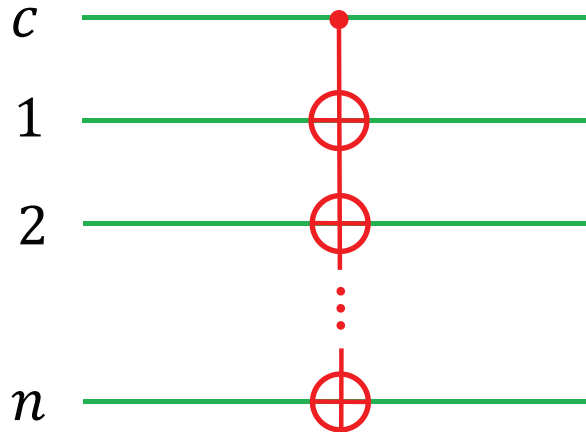
arXiv:2208.13118v1 [quant-ph] 28 Aug 2022

FIG. 1: (color online) Schematic circuit of a hybrid multi-target-qubit gate. Here, c represents the control SC qubit, while $1, 2, ..., n$ represent the n cat-state qubits. The two logic states of the SC qubit are represented by the two lowest levels $|g\rangle$ and $|e\rangle$ of a three-level SC qutrit, while the two logic states of each target cat-state qubit are represented by the two quasi-orthogonal cat states $|0\rangle$ and $|1\rangle$ (see equation (1) in the text). In the circuit, the symbol $\oplus$ represents a NOT gate on each target cat-state qubit. If the control SC qubit is in the state $|e\rangle$, then the state at $\oplus$ for each target cat-state qubit is bit flipped as $|0\rangle \rightarrow |1\rangle$ and $|1\rangle \rightarrow |0\rangle$. However, when the control SC qubit is in the state $|g\rangle$, the state at $\oplus$ for each target cat-state qubit remains unchanged.

with cat-state qubits [47-52], implementing a multi-qubit Mølmer-Sørensen *entangling* gate using cat-state qubits [53], and realizing a multi-target-qubit controlled-phase gate of cat-state qubits [54]. Schemes have also been proposed for creating *non-hybrid* Greenberger-Horne-Zeilinger (GHZ) entangled states of cat-state qubits [55,53], preparing *W*-type entangled states of cat-state qubits [56], and transferring entangled states of cat-state qubits [57]. In addition, fault-tolerant quantum computation [58,59] and holonomic geometric quantum control [60] of cat-state qubits have been studied. Moreover, experiments have demonstrated a set of single-cat-state-qubit gates [61,62] and produced entangled Bell states of two cat-state qubits [63].

The focus of this work is on hybrid quantum gates acting on different types of qubits. Hybrid quantum gates have recently drawn considerable attention. They play significant roles in connecting quantum information processors with qubits of different encoding and have important applications in the transmission of quantum states between a quantum processor and a quantum memory. Over the past years, based on cavity or circuit QED, theoretical proposals have been presented for implementing a hybrid two-qubit controlled-phase or controlled-NOT gate with a charge qubit and an atomic qubit [64], a charge qubit and a cat-state qubit [65], a photonic qubit and a SC qubit [66], a photonic qubit and a cat-state qubit [67,68], and so on. However, after a deep search of literature, we find that how to implement a *hybrid* multiqubit quantum gate with SC qubits and cat-state qubits has not been investigated yet. The hybrid multiqubit gates of SC qubits and cat-state qubits are of significance in realizing a large-scale QIP executed in a compounded information processor, which is composed of a SC-qubit based quantum processor and a cat-state-qubit based quantum processor. They are also important in the transmission of quantum states between a SC-qubit based quantum processor and a cat-state-qubit based quantum memory. Recently, the architecture consisting of a SC processor and a quantum memory has been shown to provide a significant interest [69].

In the following, we will propose a method to *directly* implement a hybrid multi-target-qubit gate, i.e., a controlled-NOT gate with one SC qubit (the control qubit) simultaneously controlling multiple target cat-state qubits (Fig. 1). As is well known, a multi-target-qubit quantum gate plays important roles in QIP. For instance, a multi-target-qubit quantum gate has applications in entanglement preparation [70], quantum cloning [71], error correction [72], and quantum algorithms [73]. Traditionally, a multi-target-qubit gate can in principle be constructed by using single-qubit and two-qubit basic gates [74,75]. However, the number of single-qubit and two-qubit gates, required to construct a multi-target-qubit gate, increases substantially with the number of qubits. As a result, the gate operation time will be quite long and decoherence significantly degrades the gate fidelity. Therefore, it is worth finding effective ways to *directly* implement multi-target-qubit quantum gates. We should point out that over the past years, many efficient methods have been proposed to directly realize multi-target-qubit gates in various physical systems [54,76-80]. However, it is noted that the previous works [54,76-80] focus on the implementation of a *non-hybrid* multi-target-qubit gate. They are different from the present work which aims at implementing a *hybrid* multi-target-qubit gate .

As an application of the proposed hybrid multi-target-qubit gate, we further discuss the generation of hybrid

GHZ entangled states of SC qubits and cat-state qubits. We also numerically analyze the experimental feasibility of preparing a hybrid GHZ entangled state of one SC qubit and three cat-state qubits within present-day circuit QED. This proposal is quite general and can be extended to implement a hybrid controlled-NOT gate with one matter qubit (e.g., an atomic qubit, a quantum dot qubit, an NV center qubit, or a SC qubit of different type) simultaneously controlling multiple target cat-state qubits in a wide range of physical systems, such as multiple microwave or optical cavities coupled to a three-level natural or artificial atom (e.g., an atom, a quantum dot, an NV center, or a SC qutrit of different type).

We stress that this work is different from Ref. [54] in the following aspects. First, Ref. [54] discussed how to implement a *non-hybrid* controlled-phase gate with one cat-state qubit simultaneously controlling multiple target cat-state qubits, while the present work focuses on the implementation of a *hybrid* controlled-NOT gate with one SC qubit simultaneously controlling multiple target cat-state qubits. The control qubit in [54] is a cat-state qubit, but the control qubit in this work is a SC qubit. Second, the gate in [54] was implemented by a pairwise cavity-cavity interaction (see the effective Hamiltonian described by Eq. (7) in [54]); In contrast, the present gate is realized by an interaction between each cavity and the coupler SC qutrit (see the effective Hamiltonian given in Eq. (6) below). Therefore, the focuses of the two works and the physical mechanisms used in the two works are different.

We would like to point out that our work is different from Ref. [53]. First, our work is for the implementation of a hybrid controlled-NOT gate with one SC qubit simultaneously controlling n target cat-state qubits, while Ref. [53] is for the realization of a multi-qubit Mølmer-Sørensen *entangling* gate using cat-state qubits. Our gate operates within a large 2^{n+1}-dimensional Hilbert space, while the entangling gate in [53] is manipulated only within a two-dimensional Hilbert space formed by two product states of cat-state qubits. Second, our gate implementation does not require the use of a classical pulse, while the gate realization in [53] requires applying a classical pulse to each cavity in order to obtain a two-photon drive on each cavity. Last, the effective Hamiltonian used for the gate realization in our work is different from the effective Hamiltonian applied for the gate implementation in [53] (see Eq. (2) there).

This paper is organized as follows. In Sec. II, we briefly introduce a hybrid controlled-NOT gate with one SC qubit simultaneously controlling multiple target cat-state qubits. In Sec. III, we explicitly show how to realize this hybrid multi-target-qubit gate. In Sec. IV, we show how to generate *hybrid* GHZ entangled states of SC qubits and cat-state qubits by applying this gate. In Sec. V, we give a discussion on the experimental feasibility of creating a hybrid GHZ state of one SC qubit and three cat-state qubits by employing three 1D microwave cavities coupled to a SC transmon qutrit. A concluding summary is given in Sec. VI.

II. HYBRID CONTROLLED-NOT GATE WITH A SC QUBIT SIMULTANEOUSLY CONTROLLING MULTIPLE TARGET CAT-STATE QUBITS

In this work, we will propose a method to realize a hybrid controlled-NOT gate with one SC qubit simultaneously controlling n target cat-state qubits $(1, 2, ..., n)$ (Fig. 1). This multi-target-qubit gate is implemented using n microwave cavities $(1, 2, ..., n)$ coupled to a SC qutrit (Fig. 2a). In our proposal, the two logic states of the SC qubit (the control qubit) are represented by the two lowest levels $|g\rangle$ and $|e\rangle$ of the SC qutrit, while the two logic states of each target cat-state qubit are represented by two quasi-orthogonal cat states of a microwave cavity. Namely, for cat-state qubit j, the two logical states $|0\rangle_j$ and $|1\rangle_j$ are encoded with two cat states of cavity j, i.e.,

$$
\begin{aligned}
|0\rangle_j &= N_\alpha(|\alpha\rangle_j + |-\alpha\rangle_j), \\
|1\rangle_j &= N_\alpha(|i\alpha\rangle_j + |-i\alpha\rangle_j),
\end{aligned}
\tag{1}
$$

where $N_\alpha = 1/\sqrt{2(1 + e^{-2|\alpha|^2})}$ is the normalization coefficient, $|\pm\alpha\rangle$ and $|\pm i\alpha\rangle$ are coherent states with a real number α. By taking α large enough, the two cat states $|0\rangle_j$ and $|1\rangle_j$ are quasi-orthogonal to each other (e.g., for $\alpha = 1.25$, one has $_j\langle 0| 1\rangle_j = \cos\alpha^2/\cosh\alpha^2 < 10^{-3}$).

For n target qubits, there exist 2^n computational basis states, which form a set of complete orthogonal bases in a 2^n-dimensional Hilbert space of the n qubits. An n-target-qubit computational basis state is denoted as $|l_1\rangle |l_2\rangle ... |l_n\rangle$, where subscripts $1, 2, ..., n$ represent target qubits $1, 2, ..., n$ respectively, and $l_j \in \{0, 1\}$ $(j = 1, 2, ..., n)$. In the present case that each target qubit is a cat-state qubit, the two logic basis states $|0\rangle_j$ and $|1\rangle_j$ of target qubit j $(j = 1, 2, ..., n)$ are encoded as shown in Eq. (1). The hybrid controlled-NOT gate, with one SC qubit simultaneously controlling n target cat-state qubits, is characterized by the following state transformation:

$$
\begin{aligned}
|g\rangle |l_1\rangle |l_2\rangle ... |l_n\rangle &\rightarrow |g\rangle |l_1\rangle |l_2\rangle ... |l_n\rangle, \\
|e\rangle |l_1\rangle |l_2\rangle ... |l_n\rangle &\rightarrow |e\rangle |\bar{l}_1\rangle |\bar{l}_2\rangle ... |\bar{l}_n\rangle,
\end{aligned}
\tag{2}
$$

where $\bar{l}_j = 1 - l_j \in \{0, 1\}$ $(j = 1, 2, ..., n)$. This transformation (2) implies that only when the control SC qubit (the first qubit) is in the state $|e\rangle$, a bit flip happens to the state of each of the n target cat-state qubits, i.e., $|0\rangle \rightarrow |1\rangle$ and $|1\rangle \rightarrow |0\rangle$ for each target cat-state qubit, while nothing happens to the state of each target cat-state qubit when the
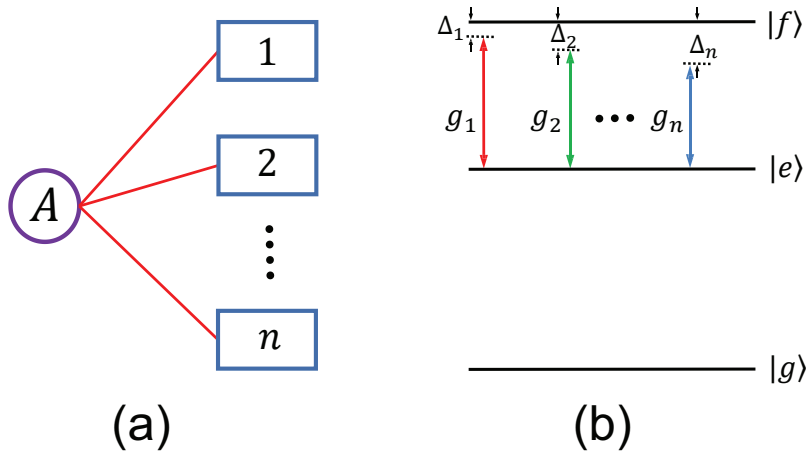
FIG. 2: (color online) (a) Schematic circuit of n microwave cavities coupled to a SC qutrit. Each square represents a one-dimensional (1D) or three-dimensional (3D) microwave cavity. The circle A represents the SC qutrit, which is inductively or capacitively coupled to each cavity. (b) Illustration of n cavities $(1, 2, ..., n)$ dispersively coupled to the $|e\rangle \leftrightarrow |f\rangle$ transition of the qutrit. In (b), the level spacing between the upper two levels is smaller than that between the two lowest levels, which applies to a SC phase, transmon, Xmon, or fluxonium qutrit. Alternatively, the level spacing between the upper two levels can be larger than that between the two lowest levels, which applies to a SC charge, flux, or fluxonium qutrit, etc..

control SC qubit is in the state $|g\rangle$. In the next section, we will show how to implement this hybrid multi-target-qubit gate.

III. IMPLEMENTATION OF THE HYBRID MULTI-TARGET-QUBIT CONTROLLED-NOT GATE

The physical system consists of n microwave cavities $(1, 2, ..., n)$ coupled to a SC qutrit (Fig. 2a). We define the three levels of the qutrit as $|g\rangle$, $|e\rangle$ and $|f\rangle$ (Fig. 2b). Suppose that cavity j $(j = 1, 2, ..., n)$ is dispersively coupled to the $|e\rangle \leftrightarrow |f\rangle$ transition of the qutrit with coupling constant g_j and detuning Δ_j (Fig. 2b). In addition, assume that the couplings of each cavity with the $|g\rangle \leftrightarrow |e\rangle$ and $|g\rangle \leftrightarrow |f\rangle$ transitions of the qutrit are not considered in our theoretical model. Note that the coupling and decoupling between the SC qutrit and each cavity can in principle be achieved by prior adjustment of the level spacings of the coupler qutrit or/and prior adjustment of the cavity frequency. For a SC qutrit, the level spacings can be rapidly (within 1-3 ns) adjusted by changing external control parameters (e.g., magnetic flux applied to the superconducting loop of a SC qutrit [12-14,18,81]). Moreover, the frequency of a microwave cavity or resonator can be quickly tunned within a few nanoseconds [82,83].

When the above assumptions are applied, the Hamiltonian of the entire system, in the interaction picture and after making the rotating-wave approximation (RWA), is given by (in units of $\hbar = 1$)

$$H_{\mathrm{I}} = \sum_{j=1}^{n} g_j (e^{i\Delta_j t} \hat{a}_j |f\rangle\langle e| + \mathrm{h.c.}), \tag{3}$$

where $\hat{a}_j$ is the photon annihilation operator of cavity j, and $\Delta_j = \omega_{fe} - \omega_{c_j}$. Here, ω_{fe} is the $|e\rangle \leftrightarrow |f\rangle$ transition frequency of the qutrit while ω_{c_j} is the frequency of cavity j $(j = 1, 2, ..., n)$.

In the case of $|\Delta_j| \gg g_j$ (large-detuning condition), the energy exchange does not happen between the qutrit and cavity j $(j = 1, 2, ..., n)$. In addition, when

$$\frac{|\Delta_j - \Delta_k|}{|\Delta_j^{-1}| + |\Delta_k^{-1}|} \gg g_j g_k, \tag{4}$$

(where $j, k \in \{1, 2, ..., n\}$, $j \neq k$), the qutrit does not induce the interaction between any two of the cavities. Under these considerations, it is straightforward to show that the Hamiltonian (3) becomes [84-86]

$$H_{\mathrm{e}} = -\sum_{j=1}^{n} \lambda_j (\hat{a}_j^+ \hat{a}_j |e\rangle\langle e| - \hat{a}_j \hat{a}_j^+ |f\rangle\langle f|), \tag{5}$$

where $\lambda_j = g_j^2/\Delta_j$. In Eq. (5), the first (second) term describes the photon-number dependent Stark shift of the energy level $|e\rangle$ ($|f\rangle$), induced by the cavities. In the case when the level $|f\rangle$ is not occupied, the Hamiltonian (5) further reduces to

$$H_e = -\sum_{j=1}^{n} \lambda_j \hat{a}_j^+ \hat{a}_j |e\rangle\langle e|. \tag{6}$$

We set $\lambda_j = \lambda$ ($j = 1, 2, ..., n$), i.e., $\lambda_1 = \lambda_2 = ... = \lambda_n$ which turns out into

$$g_1^2/\Delta_1 = g_2^2/\Delta_2 = ... = g_n^2/\Delta_n. \tag{7}$$

Because of $\Delta_j = \omega_{fe} - \omega_{c_j}$, this equality (7) can be met by carefully selecting the detuning Δ_j via tuning the frequency ω_{c_j} of cavity j ($j = 1, 2, ..., n$).

For the Hamiltonian H_e given in Eq. (6), the unitary operator $U = e^{-iH_e t}$ can be written as

$$U = \prod_{j=1}^{n} U_j, \tag{8}$$

where U_j is a unitary operator acting on cavity j and the qutrit, which is given by

$$U_j = \exp\left(i\lambda \hat{a}_j^+ \hat{a}_j |e\rangle\langle e|t\right). \tag{9}$$

Based on Eq. (1) and Eq. (9), it is straightforward to show that the unitary operator U_j results in the following state transformation

$$\begin{aligned}
U_j|g\rangle|0\rangle_j &= |g\rangle|0\rangle_j, \\
U_j|g\rangle|1\rangle_j &= |g\rangle|1\rangle_j, \\
U_j|e\rangle|0\rangle_j &= |e\rangle N_\alpha(|e^{i\lambda t}\alpha\rangle_j + |-e^{i\lambda t}\alpha\rangle_j), \\
U_j|e\rangle|1\rangle_j &= |e\rangle N_\alpha(|e^{i\lambda t}i\alpha\rangle_j + |-e^{i\lambda t}i\alpha\rangle_j).
\end{aligned} \tag{10}$$

For $\lambda t = \pi/2$, we have

$$\begin{aligned}
N_\alpha\left(|e^{i\lambda t}\alpha\rangle_j + |-e^{i\lambda t}\alpha\rangle_j\right) &= N_\alpha\left(|i\alpha\rangle_j + |-i\alpha\rangle_j\right) = |1\rangle_j, \\
N_\alpha\left(|e^{i\lambda t}i\alpha\rangle_j + |-e^{i\lambda t}i\alpha\rangle_j\right) &= N_\alpha\left(|-\alpha\rangle_j + |\alpha\rangle_j\right) = |0\rangle_j.
\end{aligned} \tag{11}$$

Based on Eq. (11), the state transformation (10) thus becomes

$$\begin{aligned}
U_j|g\rangle|0\rangle_j &= |g\rangle|0\rangle_j, \\
U_j|g\rangle|1\rangle_j &= |g\rangle|1\rangle_j, \\
U_j|e\rangle|0\rangle_j &= |e\rangle|1\rangle_j, \\
U_j|e\rangle|1\rangle_j &= |e\rangle|0\rangle_j,
\end{aligned} \tag{12}$$

which implies that when the SC qubit is initially in the state $|e\rangle$, the state $|0\rangle_j$ ($|1\rangle_j$) of cat-state qubit j flips to the state $|1\rangle_j$ ($|0\rangle_j$); otherwise, nothing happens to the state of cat-state qubit j when the SC qubit is initially in the state $|g\rangle$.

According to Eqs. (8) and (12), it is easy to obtain the following state transformation

$$\begin{aligned}
\prod_{j=1}^{n} U_j |g\rangle |l_1\rangle |l_2\rangle ... |l_n\rangle &= |g\rangle |l_1\rangle |l_2\rangle ... |l_n\rangle, \\
\prod_{j=1}^{n} U_j |e\rangle |l_1\rangle |l_2\rangle ... |l_n\rangle &= |e\rangle |\bar{l}_1\rangle |\bar{l}_2\rangle ... |\bar{l}_n\rangle,
\end{aligned} \tag{13}$$

where $l_j, \bar{l}_j \in \{0, 1\}$, and $\bar{l}_j = 1 - l_j$ ($j = 1, 2, ..., n$).

The result (13) shows that when the control SC qubit is in the state $|g\rangle$, nothing happens to the state of each of the n target cat-state qubits ($1, 2, ..., n$); however, when the control SC qubit is in the state $|e\rangle$, a bit flip from $|0\rangle$ to $|1\rangle$ (from $|1\rangle$ to $|0\rangle$) happens to the state $|0\rangle$ ($|1\rangle$) of each of the n target cat-state qubits ($1, 2, ..., n$). Hence, a hybrid
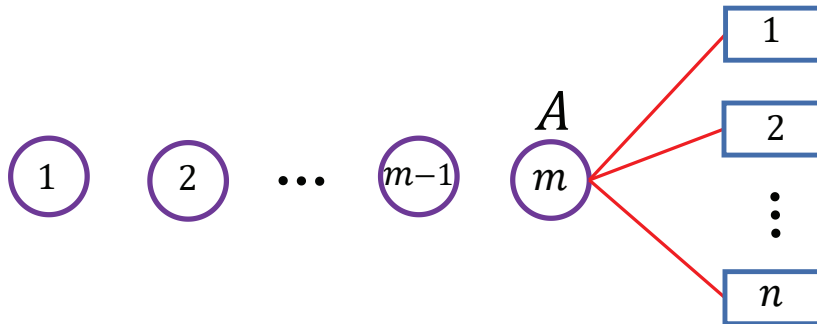
FIG. 3: (color online) Schematic of setup of m SC qubits $(1, 2, ..., m)$ and n microwave cavities $(1, 2, ..., n)$. Here, the mth SC qubit is formed by the two lowest levels of a SC qutrit A (see Fig. 2b), which is coupled to the n cavities. Note that the remaining $m - 1$ SC qubits $(1, 2, ..., m - 1)$ are decoupled from the n cavities. The $m - 1$ circles on the left represent the $m - 1$ SC qubits $(1, 2, ..., m - 1)$, while the rightmost circle represents the mth SC qubit or the coupler qutrit A. Eeach square represents a 1D or 3D microwave cavity.

multi-target-qubit controlled-NOT gate, described by Eq. (2), is implemented with a SC qubit (the control qubit) and n target cat-state qubits $(1, 2, ..., n)$, after the above operation.

As shown above, this hybrid multi-target-qubit gate is realized through a single unitary operator U. Note that we derived the unitary operator U by starting with the original Hamiltonian (3). Therefore, the gate realization only requires a single-step operation described by U. The third higher energy level $|f\rangle$ of the qutrit is not occupied during the gate operation. Thus, decoherence from this level of the qutrit is greatly suppressed. In addition, neither applying a classical pulse to the qutrit nor performing a measurement on the state of the qutrit/ cavities is needed for the gate realization.

IV. GENERATION OF HYBRID GHZ ENTANGLED STATES

Hybrid entangled states play a key role in QIP and quantum technology. For example, they help to answer fundamental questions, such as the boundary between quantum and classical domains, and the so-called Schrödinger's paradox [87], where microscopic quantum systems and macroscopic classical systems are entangled with each other. Moreover, hybrid entangled states can be used as an important quantum channel and intermediate resource for quantum technology, covering the transmission, operation, and storage of quantum information between different formats and encodings [88-90]. On the other hand, GHZ entangled states are not only of great interest for fundamental tests of quantum mechanics [91], but also have applications in QIP [92], quantum communications[93], error-correction protocols [94], quantum metrology [95], and high-precision spectroscopy [96]. In this section, we discuss how to create a hybrid GHZ entangled state of SC qubits and cat-state qubits by applying the gate above.

A. Generation of hybrid GHZ entangled states with *one* SC qubit and n cat-state qubits

Let us return to the physical system depicted in Fig. 2a. Assume that the SC qutrit is initially in the state $|+\rangle = (|g\rangle + |e\rangle)/\sqrt{2}$, which can be readily prepared by applying a classical pulse (resonant with the $|g\rangle \leftrightarrow |e\rangle$ transition) to the qutrit in the ground state $|g\rangle$ [97]. In addition, assume that each cavity is initially in the cat state $|0\rangle = N_\alpha(|\alpha\rangle + |-\alpha\rangle)$. Experimentally, the cat state here has been produced in circuit QED [62,98-101]. The initial state of the whole system is thus given by

$$|\psi(0)\rangle = \frac{1}{\sqrt{2}}(|g\rangle + |e\rangle)|0\rangle_1|0\rangle_2...|0\rangle_n. \tag{14}$$

Now apply the hybrid controlled-NOT gate (13) [i.e., the gate in Eq. (2)] on the qutrit and the n cat-state qubits. According to Eq. (13), it is easy to see that the state $|\psi(0)\rangle$ becomes

$$|\text{GHZ}\rangle_{\text{hyb}} = \frac{1}{\sqrt{2}}(|g\rangle|0\rangle_1|0\rangle_2...|0\rangle_n + |e\rangle|1\rangle_1|1\rangle_2...|1\rangle_n), \tag{15}$$

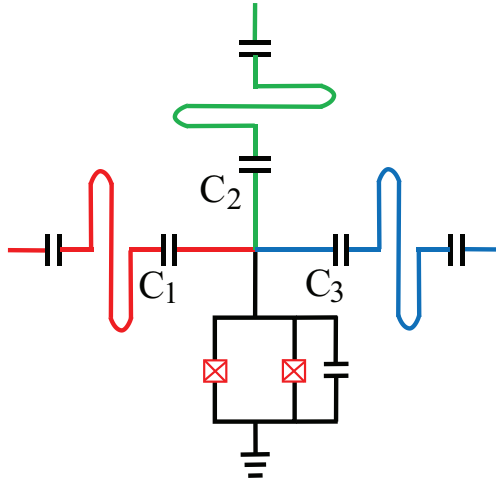which shows that one SC qubit and n cat-state qubits are prepared in a hybrid GHZ entangled state.

FIG. 4: (color online) Diagram of three 1D microwave cavities capacitively coupled to a SC transmon qutrit. Each cavity here is a one-dimensional transmission line resonator. The transmon qutrit consists of two Josephson junctions and a capacitor.

B. Generation of hybrid GHZ entangled states with m SC qubits and n cat-state qubits

Let us consider m SC qubits $(1, 2, ..., m)$ and n microwave cavities $(1, 2, ..., n)$. The n cavities are coupled to a SC qutrit A (Fig. 3). Note that the mth SC qubit here are formed by the two lowest levels of the coupler SC qutrit A. Assume that each cavity is initially in the cat state $|0\rangle = N_\alpha(|\alpha\rangle + |-\alpha\rangle)$. In addition, assume that the m SC qubits $(1, 2, ..., m)$ are initially in the GHZ state $|GHZ\rangle = (|g\rangle_1|g\rangle_2...|g\rangle_m + |e\rangle_1|e\rangle_2...|e\rangle_m)/\sqrt{2}$. In the past years, theoretical schemes for preparing multi-SC-qubit GHZ entangled states have been proposed [102-107], and the experimental production of GHZ entangled states with up to 18 SC qubits has been reported [12,18,19,30-34]. The initial state of the whole system is thus given by

$$|\psi(0)\rangle' = \frac{1}{\sqrt{2}}\left(|g\rangle_1|g\rangle_2...|g\rangle_m + |e\rangle_1|e\rangle_2...|e\rangle_m\right)|0\rangle_1|0\rangle_2...|0\rangle_n. \tag{16}$$

The first $m-1$ SC qubits $(1, 2, ..., m-1)$ are not coupled to the n cavities, while the mth SC qubit (i.e., the coupler SC qutrit A) is dispersively coupled to the n cavities such that a hybrid controlled-NOT gate (13) is performed on the mth SC qubit and the n cat-state qubits. The details on the implementation of the gate (13) are presented in the previous section III. According to Eq. (13), it is easy to see that after the gate operation, the state $|\psi(0)\rangle'$ becomes

$$|GHZ\rangle_{\text{hyb}} = \frac{1}{\sqrt{2}}\left(g\rangle_1|g\rangle_2...|g\rangle_{m-1}|g\rangle_m|0\rangle_1|0\rangle_2...|0\rangle_n|g\rangle + |e\rangle_1|e\rangle_2...|e\rangle_{m-1}|e\rangle_m|1\rangle_1|1\rangle_2...|1\rangle_n\right), \tag{17}$$

which shows that the m SC qubits $(1, 2, ..., m)$ and the n cat-state qubits $(1, 2, ..., n)$ are prepared in a hybrid GHZ entangled state.

From the descriptions given above, one can see that the hybrid GHZ states of SC qubits and cat-state qubits can be straightfowardly created by applying the hybrid controlled-NOT gate (2) or (13). Given that the initial state $|\psi(0)\rangle$ or $|\psi(0)\rangle'$ of the system is ready, the operation time for the preparation of the hybrid GHZ state (15) or (17) is equal to that for the implementation of the gate (13), i.e., $t = \pi/(2\lambda)$. Since the GHZ states here are created based on the gate (13), the Hamiltonians used for the GHZ state production are the same as those used for the implementation of the gate (13).

Before ending this section, it should be mentioned that both Refs. [53,55] have proposed how to create *non-hybrid* GHZ entangled states of multiple cat-state qubits. However, it is noted that how to prepare a *hybrid* GHZ entangled state with SC qubits and cat-state qubits was not studied in both of [53,55].

V. POSSIBLE EXPERIMENTAL IMPLEMENTATION

In this section, as an example, we investigate the experimental feasibility for creating a hybrid GHZ state with one SC qubit and three cat-state qubits [i.e., the GHZ state (15) with $n = 3$], by using three 1D microwave cavities coupled to a SC transmon qutrit (Fig. 4). As shown in subsection IV A, the GHZ state (15) was prepared by applying
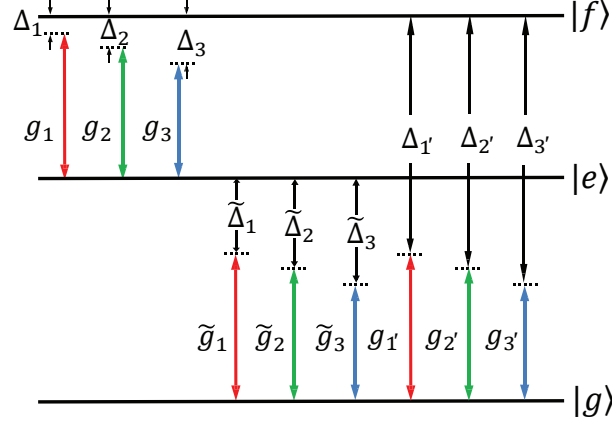
FIG. 5: (color online) Illustration of three cavities (1,2,3) coupled to the $|e\rangle \leftrightarrow |f\rangle$ transition of the qutrit, as well as the unwanted couplings of the three cavities with the $|g\rangle \leftrightarrow |f\rangle$ transition and the $|g\rangle \leftrightarrow |e\rangle$ transition of the qutrit.

the hybrid multi-target-qubit controlled-NOT gate (13) [i.e., the gate in Eq. (2)]. In this sense, as long as the initial state (14) can be well prepared, the operational fidelity for the preparation of the GHZ state (15) mainly depends on the performance of the hybrid gate (13) applied on the SC qubit and the three cat-state qubits.

A. Full Hamiltonian

In the preceding section III, the hybrid gate (13) was realized based on the effective Hamiltonian (6). Note that this Hamiltonian was derived from the original Hamiltonian (3), which only contains the coupling between each cavity and the $|e\rangle \leftrightarrow |f\rangle$ transition of the SC qutrit. In a realistic situation, there exists the unwanted coupling between each cavity and the $|g\rangle \leftrightarrow |f\rangle$ transition of the SC qutrit as well as the unwanted coupling between each cavity and the $|g\rangle \leftrightarrow |e\rangle$ transition of the SC qutrit. In addition, there exists the unwanted inter-cavity crosstalk between the three cavities.

By taking the unwanted couplings and the unwanted inter-cavity crosstalk into account, the Hamiltonian (3), with $n = 3$ for the present case, is modified as

$$
\begin{aligned}
H'_{\mathrm{I}} = {} & \sum_{j=1}^{3} g_j (e^{i\Delta_j t} \hat{a}_j |f\rangle\langle e| + \text{h.c.}) \\
& + \sum_{j=1}^{3} g'_j (e^{i\Delta'_j t} \hat{a}_j |f\rangle\langle g| + \text{h.c.}) + \sum_{j=1}^{3} \widetilde{g}_j (e^{i\widetilde{\Delta}_j t} \hat{a}_j |e\rangle\langle g| + \text{h.c.}) \\
& + \left(g_{12} e^{i\Delta_{12} t} \hat{a}_1^+ \hat{a}_2 + \text{h.c.} \right) + \left(g_{13} e^{i\Delta_{13} t} \hat{a}_1^+ \hat{a}_3 + \text{h.c.} \right) + \left(g_{23} e^{i\Delta_{23'} t} \hat{a}_2^+ \hat{a}_3 + \text{h.c.} \right),
\end{aligned}
\tag{18}
$$

where the term in line one represents the required coupling of cavity j with $|e\rangle \leftrightarrow |f\rangle$ transition of the SC qutrit (Fig. 5), the first term in line two represents the unwanted coupling of cavity j with $|g\rangle \leftrightarrow |f\rangle$ transition of the SC qutrit with the coupling constant g'_j and the detuning $\Delta'_j = \omega_{fg} - \omega_{c_j}$ (Fig. 5), the second term in line two represents the unwanted coupling of cavity j with $|g\rangle \leftrightarrow |e\rangle$ transition of the SC qutrit with the coupling constant $\widetilde{g}_j$ and the detuning $\widetilde{\Delta}_j = \omega_{eg} - \omega_{c_j}$ (Fig. 5), while the terms in the last line represent the unwanted inter-cavity crosstalk among the three cavities, g_{kl} is the crosstalk strength between the two cavities k and l with the frequency difference $\Delta_{kl} = \omega_{c_k} - \omega_{c_l}$ ($k, l \in \{1, 2, 3\}; k \neq l$). Here, ω_{fg} (ω_{eg}) is the $|g\rangle \leftrightarrow |f\rangle$ ($|g\rangle \leftrightarrow |e\rangle$) transition frequency of the qutrit, while ω_{c_k} (ω_{c_l}) is the frequency of cavity k (l).

B. Numerical results

The dynamics of the lossy system, with finite qutrit relaxation, dephasing and photon lifetime being included, is

$\omega_{eg}/2\pi = 4.0\,\text{GHz}$	$\omega_{fe}/2\pi = 3.3\,\text{GHz}$	$\omega_{fg}/2\pi = 7.3\,\text{GHz}$
$\omega_{c_1}/2\pi = 3.24\,\text{GHz}$	$\omega_{c_2}/2\pi = 3.21\,\text{GHz}$	$\omega_{c_3}/2\pi = 3.18\,\text{GHz}$
$\triangle_1/2\pi = 60\,\text{MHz}$	$\triangle_2/2\pi = 90\,\text{MHz}$	$\triangle_3/2\pi = 120\,\text{MHz}$
$\triangle_{1'}/2\pi = 4.06\,\text{GHz}$	$\triangle_{2'}/2\pi = 4.09\,\text{GHz}$	$\triangle_{3'}/2\pi = 4.12\,\text{GHz}$
$\widetilde{\triangle}_1/2\pi = 760\,\text{MHz}$	$\widetilde{\triangle}_2/2\pi = 790\,\text{MHz}$	$\widetilde{\triangle}_3/2\pi = 820\,\text{MHz}$
$\triangle_{12}/2\pi = 30\,\text{MHz}$	$\triangle_{23}/2\pi = 30\,\text{MHz}$	$\triangle_{13}/2\pi = 60\,\text{MHz}$
$g_1/2\pi = 4.5\,\text{MHz}$	$g_2/2\pi = 5.51\,\text{MHz}$	$g_3/2\pi = 6.36\,\text{MHz}$

TABLE I: For the definitions of the parameters, please refer to the text. Except for g_2 and g_3, all parameters listed are used in the numberical simulations for plotting Figs. 6 and 7. The coupling constants g_2 and g_3 listed are used for Fig. 6, which are calculated according to Eq. (7). While, the coupling constants g_2 and g_3 used for Fig. 7 are not shown, which are dependent of c [see Eq. (21)] and calculated according to Eq. (21), by using the values of g_1, Δ_1, Δ_2, and Δ_3 listed in the table.

determined by

$$
\begin{aligned}
\frac{d\rho}{dt} = {} & -i\left[H'_{\text{I}}, \rho\right] + \sum_{j=1}^{3} \kappa_j \mathcal{L}\left[\hat{a}_j\right] \\
& + \gamma_{eg}\mathcal{L}\left[\sigma_{eg}^-\right] + \gamma_{fe}\mathcal{L}\left[\sigma_{fe}^-\right] + \gamma_{fg}\mathcal{L}\left[\sigma_{fg}^-\right] \\
& + \gamma_{e,\varphi}\left(\sigma_{ee}\rho\sigma_{ee} - \sigma_{ee}\rho/2 - \rho\sigma_{ee}/2\right) \\
& + \gamma_{f,\varphi}\left(\sigma_{ff}\rho\sigma_{ff} - \sigma_{ff}\rho/2 - \rho\sigma_{ff}/2\right),
\end{aligned}
\tag{19}
$$

where $\sigma_{eg}^- = |g\rangle\langle e|$, $\sigma_{fe}^- = |e\rangle\langle f|$, $\sigma_{fg}^- = |g\rangle\langle f|$, $\sigma_{ee} = |e\rangle\langle e|$, $\sigma_{ff} = |f\rangle\langle f|$, $\mathcal{L}[\Lambda] = \Lambda\rho\Lambda^+ - \Lambda^+\Lambda\rho/2 - \rho\Lambda^+\Lambda/2$ (with $\Lambda = \hat{a}_j, \sigma_{eg}^-, \sigma_{fe}^-, \sigma_{fg}^-)$, κ_j is the decay rate of cavity j ($j = 1, 2, 3$), γ_{eg} is the energy relaxation rate of the level $|e\rangle$ for the decay path $|e\rangle \rightarrow |g\rangle$ of the qutrit, γ_{fe} (γ_{fg}) is the relaxation rate of the level $|f\rangle$ for the decay path $|f\rangle \rightarrow |e\rangle$ ($|f\rangle \rightarrow |g\rangle$) of the qutrit; $\gamma_{e,\varphi}$ ($\gamma_{f,\varphi}$) is the dephasing rate of the level $|e\rangle$ ($|f\rangle$) of the qutrit.

The operational fidelity is given by $F = \sqrt{\langle\psi_{\text{id}}|\rho|\psi_{\text{id}}\rangle}$, where $|\psi_{\text{id}}\rangle$ is the ideal output state of Eq. (15) with $n = 3$ (which is obtained without considering the system dissipation, the inter-cavity crosstalk and the unwanted couplings); while ρ is the density operator of the system when the operation is performed in a realistic situation.

As a concrete example, let us consider the parameters listed in Table 1, which are used in our numerical simulations. For a transmon qutrit, the level spacing anharmonicity 100-720 MHz was reported in experiments [108]. For a transmon qutrit [109], one has $\widetilde{g}_j = g_j/\sqrt{2}(j = 1, 2, , 3)$. Since the $|g\rangle \leftrightarrow |f\rangle$ transition for a transmon qutrit is forbidden or weak [109], we choose $g'_j = 0.01g_j$ ($j = 1, 2, , 3$). For the coupling constants listed in Table 1, the maximal value $g_{\text{max}} = \max\{g_1, g_2, g_3\}$ is $2\pi \times 6.36$ MHz, which is readily available because a coupling strength $\sim 2\pi \times 360$ MHz has been reported for a transmon qutrit coupled to a 1D microwave cavity [110].

Other parameters used in the numerical simulations are: (i) $\gamma_{eg}^{-1} = 60~\mu s$, $\gamma_{fg}^{-1} = 150~\mu s$ [111], $\gamma_{fe}^{-1} = 30~\mu s$, $\gamma_{\phi e}^{-1} = \gamma_{\phi f}^{-1} = 20~\mu s$, (ii) $\kappa_1 = \kappa_2 = \kappa_3 = \kappa$, (iii) $g_{12} = g_{23} = g_{13} = g_{cr}$, (iv) $g_{cr} = 0.01g_{\text{max}}$, and (v) $\alpha = 1.25$. Here, we consider a rather conservative case for decoherence time of the transmon qutrit because energy relaxation time with a range from 65 μs to 0.5 ms and dephasing time from 25 μs to 75 μs have been experimentally demonstrated for a superconducting transmon device [8,9,112,113]. In addition, for each cavity, a cat state with $\alpha = 1.25$ can be created in experiments because the circuit-QED experimental preparation of a cat state with the amplitude $|\alpha| \leq 5.27$ has been reported [62,98-101]. The choice of $g_{cr} = 0.01g_{\text{max}}$ is obtainable in experiments by a prior design of the sample with appropriate capacitances C_1, C_2, and C_3 depicted in Fig. 4 [114].

In a realistic situation, the initial state of Eq. (14) may not be prepared perfectly. Therefore, we consider a non-ideal initial state of the system

$$
\begin{aligned}
|\psi(0)\rangle_{\text{non-ideal}} = {} & \widetilde{N}_\alpha^3 \left(\sqrt{1+\delta}|\alpha\rangle_1 + \sqrt{1-\delta}|-\alpha\rangle_1\right) \left(\sqrt{1+\delta}|\alpha\rangle_2 + \sqrt{1-\delta}|-\alpha\rangle_2\right) \\
& \left(\sqrt{1+\delta}|\alpha\rangle_3 + \sqrt{1-\delta}|-\alpha\rangle_3\right) \frac{1}{\sqrt{2}} \left(\sqrt{1+\delta}|g\rangle + \sqrt{1-\delta}|e\rangle\right),
\end{aligned}
\tag{20}
$$

where $\widetilde{N}_\alpha = 1/\sqrt{2 + 2\sqrt{1-\delta^2}e^{-2|\alpha|^2}}$. For this case, we numerically plot Fig. 6, which illustrates that the fidelity decreases with increasing of δ. Nevertheless, for $\delta \in [-0.1, 0.1]$, i.e., a 10% error in the weights of $|\alpha\rangle$ and $|-\alpha\rangle$
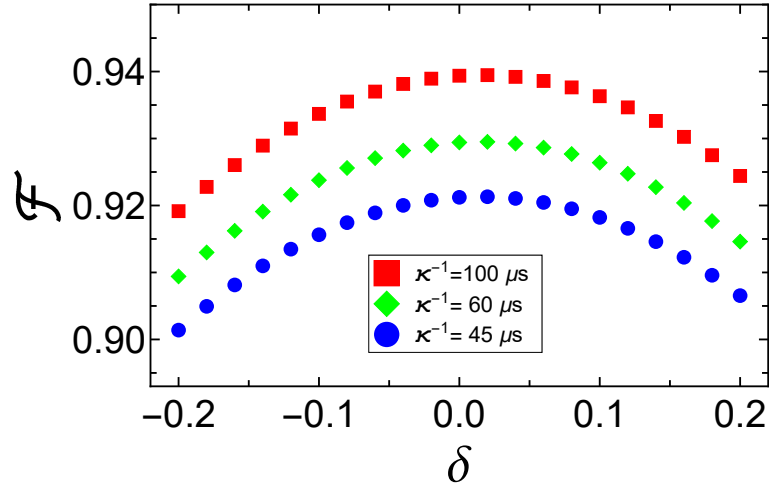
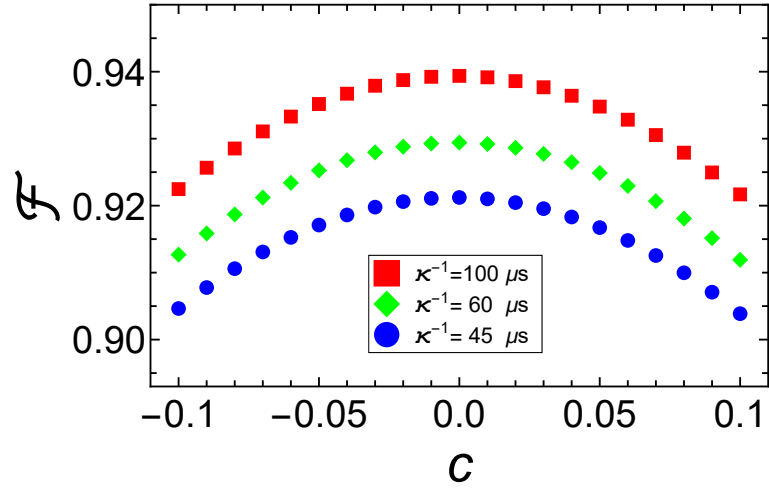FIG. 6: (color online) Fidelity versus δ for $\kappa^{-1} = 45$ μs, 60 μs, and 100 μs.

FIG. 7: (color online) Fidelity versus c for $\kappa^{-1} = 45$ μs, 60 μs, and 100 μs.

states as well as in the weights of $|g\rangle$ and $|e\rangle$, a fidelity greater than $91.56\%, 92.38\%$, and 93.37% can be achieved for $\kappa^{-1} = 45$ μs, 60 μs, 100 μs, respectively.

It may be an experimental challenge to have the condition (7) well satisfied. Thus, to be more realistic, we modify the condition (7) (with $n = 3$ for the three-cavity case) as follows:

$$g_1^2/\Delta_1 = (1 + c)\, g_2^2/\Delta_2 = (1 - c)\, g_3^2/\Delta_3. \tag{21}$$

We numerically plot Fig. 7, which illustrates the fidelity versus c. The coupling constants g_2 and g_3, used in the numerical simulation for plotting Fig. 7, are dependent of c and calculated according to Eq. (21), given the values of g_1, Δ_1, Δ_2, and Δ_3 listed in Table 1. Figure 7 shows that the fidelity decreases with increasing of c. However, for $c \in [-0.05, 0.05]$, i.e., a 5% deviation with respect to the ideal condition (7), the fidelity is greater than $91.67\%, 92.49\%$, and 93.48% for $\kappa^{-1} = 45$ μs, 60 μs, 100 μs, respectively. This result indicates that a high fidelity can still be obtained when the condition (7) is not well satisfied.

The operational time for the GHZ state preparation is estimated to be ~ 0.74 μs, which is much shorter than the decoherence time of the transmon qutrit and the cavity decay time used in the numerical simulations. For the cavity frequencies given in Table 1 and $\kappa^{-1} = 45$ μs, the quality factors of the three cavities are $Q_1 \sim 9.16 \times 10^5$, $Q_2 \sim 9.07 \times 10^5$, and $Q_3 \sim 8.99 \times 10^5$, which are available because a 1D microwave cavity or resonator with a high quality factor $Q \gtrsim 10^6$ was reported in experiments [37-42].

C. Discussion

The analysis presented above shows that the operational fidelity is sensitive to the error in the initial state preparation and the deviation from the ideal condition (7). Our numerical simulations demonstrate that a high fidelity can still be obtained when the error in the initial state preparation and the deviation from the condition (7) are small. In order to achieve a high fidelity, one would need to reduce the error in the initial state prepare, reduce the deviation from the condition (7), select cavities with a high quality factor, and choose the qutrit with a long coherence time. One can also improve the fidelity by employing a coupler qutrit with a larger level anharmonicity, so that the unwanted couplings between each cavity and the irrelevant level transitions of the qutrit are negligible. Finally, it should be remarked that further investigation is needed for each particular experimental setup. However, this requires a rather lengthy and complex analysis, which is beyond the scope of this theoretical work.

VI. CONCLUSIONS

We have proposed a one-step method to realize a *hybrid* controlled-NOT gate with one SC qubit simultaneously controlling multiple target cat-state qubits. This proposal operates essentially through the dispersive coupling of each cavity with the coupler qutrit. To the best of our knowledge, this work is the first to demonstrate the realization of the proposed hybrid multi-target-qubit gate based on cavity or circuit QED. This proposal is quite general and can be applied to implement a hybrid controlled-NOT gate with one matter qubit (of different type) simultaneously controlling multiple target cat-state qubits in a wide range of physical systems.

As shown above, this proposal has the following features and advantages: (i) The gate implementation is quite simple, because it requires only a single-step operation; (ii) Neither classical pulse nor measurement is needed; (iii) The hardware resources are significantly reduced because only one coupler SC qutrit is needed to couple all of the cavities; (iv) The intermediate higher energy level of the SC qutrit is not occupied during the gate realization, thus decoherence from the coupler SC qutrit is significantly reduced; and (v) The gate operation time is independent of the number of target qubits, thus it does not increase with an increasing number of target qubits.

As an application, we further discuss how to create a hybrid GHZ entangled state of SC qubits and cat-state qubits, by applying the proposed hybrid multi-qubit gate. To the best of our knowledge, our work is the first to show the preparation of a *hybrid* GHZ entangled state of SC qubits and cat-state qubits. We have also numerically analyzed the experimental feasibility of generating a hybrid GHZ state with one SC qubit and three cat-state qubits within current circuit QED technology. We hope that this work will stimulate experimental activities in the near future.

ACKNOWLEDGEMENTS

---

[1] C. P. Yang, S. I. Chu, and S. Han, Possible realization of entanglement, logical gates, and quantum information transfer with superconducting-quantum-interference-device qubits in cavity QED, Phys. Rev. A **67**, 042311 (2003).

[2] J. Q. You and F. Nori, Quantum information processing with superconducting qubits in a microwave field, Phys. Rev. B **68**, 064509 (2003).

[3] A. Blais, R. S. Huang, A. Wallraff, S. M. Girvin, and R. J. Schoelkopf, Cavity quantum electrodynamics for superconducting electrical circuits: An architecture for quantum computation, Phys. Rev. A **69**, 062320 (2004).

[4] J. Q. You and F. Nori, Atomic physics and quantum optics using superconducting circuits, Nature (London) **474**, 589 (2011).

[5] I. Buluta, S. Ashhab, and F. Nori, Natural and artificial atoms for quantum computation, Rep. Prog. Phys. **74**, 104401 (2011).

[6] Z. L. Xiang, S. Ashhab, J. Q. You, and F. Nori, Hybrid quantum circuits: Superconducting circuits interacting with other quantum systems, Rev. Mod. Phys. **85**, 623 (2013).

[7] X. Gu, A. F. Kockum, A. Miranowicz, Y. X. Liu, and F. Nori, Microwave photonics with superconducting quantum circuits, Phys. Rep. **718**, 1 (2017).

[8] A. P. M. Place, L. V. H. Rodgers, P. Mundada, B. M. Smitham, M. Fitzpatrick, Z. Leng, A. Premkumar, J. Bryon, A. Vrajitoarea, S. Sussman et al., New material platform for superconducting transmon qubits with coherence times exceeding 0.3 milliseconds, Nat. Commun. **12**, 1779 (2021).

[9] C. L. Wang, X. G. Li, H. K. Xu, Z. Y. Li, J. H. Wang, Z. Yang, Z. Y. Mi, X. H. Liang, T. Su, C. H. Yang et al., Transmon qubit with relaxation time exceeding 0.5 milliseconds, arXiv:2105.09890.

[10] F. Yan, S. Gustavsson, A. Kamal, J. Birenbaum, A. P. Sears, D. Hover, T. J. Gudmundsen, J. L. Yoder, T. P. Orlando, J. Clarke et al., The Flux Qubit Revisited to Enhance Coherence and Reproducibility, Nat. Commun. **7**, 12964 (2016).

[11] A. Somoroff, Q. Ficheux, R. A. Mencia, H. N. Xiong, R. Kuzmin, and V. E. Manucharyan, Millisecond coherence in a superconducting qubit, arXiv:2103.08578.

[12] P. J. Leek, S. Filipp, P. Maurer, M. Baur, R. Bianchetti, J. M. Fink, M. Goppl, L. Steffen, and A. Wallraff, Using sideband transitions for two-qubit operations in superconducting circuits, Phys. Rev. B **79**, 180511 (2009).

[13] R. Barends, J. Kelly, A. Megrant, D. Sank, E. Jeffrey, Y. Chen, Y. Yin, B. Chiaro, J. Mutus, C. Neill et al., Coherent Josephson qubit suitable for scalable quantum integrated circuits, Phys. Rev. Lett. **111**, 080502 (2013).

[14] M. Neeley, M. Ansmann, R. C. Bialczak, M. Hofheinz, N. Katz, E. Lucero, A. O'Connell, H. Wang, A. N. Cleland, and J. M. Martinis, Process tomography of quantum memory in a Josephson-phase qubit coupled to a two-level state, Nat. Phys. **4**, 523 (2008).

[15] T. Yamamoto, Y. A. Pashkin, O. Astafiev, Y. Nakamura and J. S. Tsai, Demonstration of conditional gate operation using superconducting charge qubits, Nature (London) **425**, 941 (2003).

[16] J. H. Plantenberg, P. C. de Groot, C. J. P. M. Harmans and J. E. Mooij, Demonstration of controlled-NOT quantum gates on a pair of superconducting quantum bits, Nature (London) **447**, 836 (2007).

[17] R. C. Bialczak, M. Ansmann, M. Hofheinz, E. Lucero, M. Neeley, A. D. O'Connell, D. Sank, H. Wang, J. Wenner, M. Stefen et al., Quantum process tomography of a universal entangling gate implemented with Josephson phase qubits, Nat. Phys. **6**, 409 (2010).

[18] R. Barends, J. Kelly, A. Megrant, A. Veitia, D. Sank, E. Jeffrey, T. C. White, J. Mutus, A. G. Fowler, B. Campbell et al., Superconducting quantum circuits at the surface code threshold for fault tolerance, Nature (London) **508**, 500 (2014).

[19] M. Gong, M. C. Chen, Y. R. Zheng, S. Y. Wang, C. Zha, H. Deng, Z. G. Yan, H. Rong, Y. L. Wu, S. W. Li et al., Genuine 12-qubit entanglement on a superconducting quantum processor, Phys. Rev. Lett. **122**, 110501 (2019).

[20] Y. Xu, J. Chu, J. Yuan, J. Qiu, Y. Zhou, L. Zhang, X. Tan, Y. Yu, S. Liu, J. Li et al., High-fidelity, high-scalability two-qubit gate scheme for superconducting qubits, Phys. Rev. Lett. **125**, 240503 (2020).

[21] X. Li, T. Cai, H. Yan, Z. Wang, X. Pan, Y. Ma, W. Cai, J. Han, Z. Hua, X. Han et al., Tunable Coupler for Realizing a Controlled-Phase Gate with Dynamically Decoupled Regime in a Superconducting Circuit, Phys. Rev. Appl. **14**, 024070 (2020).

[22] Y. Xu, Z. Hua, Tao Chen, X. Pan, X. Li, J. Han, W. Cai, Y. Ma, H. Wang, Y. P. Song, et al., Experimental Implementation of Universal Nonadiabatic Geometric Quantum Gates in a Superconducting Circuit, Phys. Rev. Lett. **124**, 230503 (2020).

[23] M. C. Collodo, J. Herrmann, N. Lacroix, C. K. Andersen, A. Remm, S. Lazar, J. C. Besse , T. Walter, A. Wallraff, and C. Eichler, Implementation of Conditional Phase Gates Based on Tunable ZZ Interactions, Phys. Rev. Lett. **125**, 240502 (2020).

[24] M. Ganzhorn, G. Salis, D. J. Egger, A. Fuhrer, M. Mergenthaler, C. Muller, P. Muller, S. Paredes, M. Pechal, M. Werninghaus et al., Benchmarking the noise sensitivity of different parametric two-qubit gates in a single superconducting quantum computing platform, Phys. Rev. Res. **2**, 033447 (2020).

[25] V. Negirneac, H. Ali, N. Muthusubramanian, F. Battistel, R. Sagastizabal, M. S. Moreira, J. F. Marques, W. J. Vlothuizen, M. Beekman, C. Zachariadis et al., High-fidelity controlled-Z gate with maximal intermediate leakage operating at the speed limit in a superconducting quantum processor, Phys. Rev. Lett. **126**, 220502 (2021).

[26] K. Xu, W. Ning, X. J. Huang, P. R. Han, H. K. Li, Z. B. Yang, D. N. Zheng, H. Fan, and S. B. Zheng, Demonstration of a non-Abelian geometric controlled-NOT gate in a superconducting circuit, Optica **8**, 972 (2021).

[27] Z. W. Zong, Z. H. Sun, Z. J. Z. Dong, C. X. Run, L. Xiang, Z. Zhan, Q. L. Wang, Y. Fei, Y. Z. Wu, W. Y. Jin et al., Optimization of a Controlled-Z Gate with Data-Driven Gradient-Ascent Pulse Engineering in a Superconducting-Qubit System, Phys. Rev. Appl. **15**, 064005 (2021).

[28] A. Fedorov, L. Steffffen, M. Baur, M. P. D. Silva, and A. Wallraff, Implementation of a Toffoli gate with superconducting circuits, Nature (London) **481**, 170 (2012).

[29] C. Song, S. B. Zheng, P. Zhang, K. Xu, L. Zhang, Q. Guo, W. Liu, D. Xu, H. Deng, K. Huang, D. Zheng, X. Zhu, and H. Wang, Continuous-variable geometric phase and its manipulation for quantum computation in a superconducting circuit, Nat. Commun. **8**, 1061 (2017).

[30] L. DiCarlo, M. D. Reed, L. Sun, B. R. Johnson, J. M. Chow, J. M. Gambetta, L. Frunzio, S. M. Girvin, M. H. Devoret, and R. J. Schoelkopf, Preparation and measurement of three-qubit entanglement in a superconducting circuit, Nature (London) **467**, 574 (2010).

[31] Y. P. Zhong, H. S. Chang, A. Bienfait, E. Dumur, M. H. Chou, C. R. Conner, J. Grebel, R. G. Povey, H. X. Yan, D. I. Schuster et al., Deterministic multi-qubit entanglement in a quantum network, Nature (London) **590**, 571 (2021).

[32] C. Song, K. Xu, W. Liu, C. P. Yang, S. B. Zheng, H. Deng, Q. Xie, K. Huang, Q. Guo, L. Zhang et al., 10-Qubit Entanglement and Parallel Logic Operations with a Superconducting Circuit, Phys. Rev. Lett. **119**, 180511 (2017).

[33] Z. Wang, H. K. Li, W. Feng ,X. H. Song, C. Song, W. X. Liu, Q. J. Guo, X. Zhang, H. Dong, D. N. Zheng et al., Controllable Switching between Superradiant and Subradiant States in a 10-qubit Superconducting Circuit, Phys. Rev. Lett. **124**, 013601 (2020).

[34] C. Song, K. Xu, H. Li, Y. Zhang, X. Zhang, W. Liu, Q. Guo, Z. Wang, W. Ren, J. Hao et al., Observation of multi-component atomic Schrodinger cat states of up to 20 qubits, Science **365**, 574 (2019).

[35] K. X. Wei, I. Lauer, S. Srinivasan, N. Sundaresan, D. T. McClure, D. Toyli, D. C. McKay, J. M. Gambetta, and S. Sheldon, Verifying Multipartite Entangled GHZ States via Multiple Quantum Coherences, arXiv:1905.05720.

[36] W. Chen, D. A. Bennett, V. Patel, and J. E. Lukens, Substrate and process dependent losses in superconducting thin film resonators, Supercond. Sci. Technol. **21**, 075013 (2008).

[37] P. J. Leek, M. Baur, J. M. Fink, R. Bianchetti, L. Stefen, S. Filipp, and A. Wallraf, Cavity quantum electrodynamics with separate photon storage and qubit readout modes, Phys. Rev. Lett. **104**, 100504 (2010).

[38] A. Megrant, C. Neill, R. Barends, B. Chiaro, Y. Chen, L. Feigl, J. Kelly, E. Lucero, M. Mariantoni, P. J. J. O'Malley et al., Planar superconducting resonators with internal quality factors above one million, Appl. Phys. Lett. **100**, 113510 (2012).

[39] G. Calusine, A. Melville, W. Woods, R. Das, C. Stull, V. Bolkhovsky, D. Braje, D. Hover, D. K. Kim, X. Miloshi et al., Analysis and mitigation of interface losses in trenched superconducting coplanar waveguide resonators, Appl. Phys. Lett. **112**, 062601 (2018).

[40] W. Woods, G. Calusine, A. Melville, A. Sevi, E. Golden, D. K. Kim, D. Rosenberg, J. L. Yoder, and W. D. Oliver, Determining interface dielectric losses in superconducting coplanar waveguide resonators, Phys. Rev. Appl. **12**, 014012 (2019).

[41] A. Melville, G. Calusine, W. Woods, K. Serniak, E. Golden, B. M. Niedzielski, D. K. Kim, A. Sevi, J. L. Yoder, E. A. Dauler et al., Comparison of dielectric loss in titanium nitride and aluminum superconducting resonators, Appl. Phys. Lett. **117**, 124004 (2020).

[42] M. Reagor, W. Pfaff, C. Axline, R. W. Heeres, N. Ofek, K. Sliwa, E. Holland, C. Wang, J. Blumoff, K. Chou et al., A quantum memory with near-millisecond coherence in circuit QED, Phys. Rev. B **94**, 014506 (2016).

[43] M. Kudra, J. Biznarova, A. Fadavi Roudsari, J. J. Burnett, D. Niepce, S. Gasparinetti, B. Wickman, and P. Delsing, High quality three-dimensional aluminum microwave cavities, Appl. Phys. Lett. **117**, 070601 (2020).

[44] Romanenko, R. Pilipenko, S. Zorzetti, D. Frolov, M. Awida, S. Belomestnykh, S. Posen, and A. Grassellino, Three-Dimensional Superconducting Resonators at $T < 20$ mK with Photon Lifetimes up to $\tau = 2$ s, Phys. Rev. Appl. **13**, 034032 (2020).

[45] M. H. Devoret, and R. J. Schoelkopf, Superconducting circuits for quantum information: an outlook, Science **339**, 1169 (2013).

[46] N. Ofek, A. Petrenko, R. Heeres, P. Reinhold, Z. Leghtas, B. Vlastakis, Y. Liu, L. Frunzio, S. M. Girvin, L. Jiang et al., Extending the lifetime of a quantum bit with error correction in superconducting circuits, Nature (London) **536**, 441 (2016).

[47] M. Mirrahimi, Z. Leghtas, V. V. Albert, S. Touzard, R. J. Schoelkopf, L. Jiang, and M. H. Devoret, Dynamically protected cat-qubits: a new paradigm for universal quantum computation, New J. Phys. **16**, 045014 (2014).

[48] S. E. Nigg, Deterministic hadamard gate for microwave cat-state qubits in circuit QED, Phys. Rev. A **89**, 022340 (2014).

[49] Y. Zhang, X. Zhao, Z. F. Zheng, L. Yu, Q. P. Su, and C. P. Yang, Universal controlled-phase gate with cat-state qubits in circuit QED, Phys. Rev. A **96**, 052317 (2017).

[50] S. Puri, L. St-Jean, J. A. Gross, A. Grimm, N. E. Frattini, P. S. Iyer, A. Krishna, S. Touzard, L. Jiang, A. Blais, S. T. Flammia, and S. M. Girvin, Bias-preserving gates with stabilized cat qubits, Sci. Adv. **6**, eaay5901 (2020).

[51] Q. Xu, J. K. Iverson, F. Brandão, and L. Jiang, Engineering fast bias-preserving gates on stabilized cat qubits, arXiv:2105.13908

[52] Y. H. Kang, Y. H. Chen, X. Wang, J. Song, Y. Xia, A. Miranowicz, S. B. Zheng, and F. Nori, Nonadiabatic geometric quantum computation with cat qubits via invariant-based reverse engineering, arXiv:2110.01933

[53] Y. H. Chen, R. Stassi, W. Qin, A. Miranowicz, and F. Nori, Fault-Tolerant Multi-Qubit Geometric Entangling Gates Using Photonic Cat Qubits, arXiv:2109.04643

[54] Y. J. Fan, Z. F. Zheng, Y. Zhang, D. M. Lu, and C. P. Yang, One-step implementation of a multi-target-qubit controlled phase gate with cat-state qubits in circuit QED, Front. Phys. **14**, 21602 (2019).

[55] C. P. Yang, Z. F. Zheng, Deterministic generation of GHZ entangled states of cat-state qubits in circuit QED, Opt. Lett. **43**, 5127 (2018).

[56] Y. Zhang, T. Liu, Y. Yu, and C. P. Yang, Preparation of entangled W states with cat-state qubits in circuit QED, Quantum Inf. Process. **19**, 218 (2020).

[57] T. Liu, Z. F. Zheng, Y. Zhang, Y. L. Fang, C. P. Yang, Transferring entangled states of photonic cat-state qubits in circuit QED, Front. Phys. **15**, 21603 (2020).

[58] J. Guillaud and M. Mirrahimi, Repetition cat qubits for fault-tolerant quantum computation, Phys. Rev. X **9**, 041053 (2019).

[59] C. Chamberland, K. Noh, P. Arrangoiz-Arriola, E. T. Campbell, C. T. Hann, J. Iverson, H. Putterman, T. C. Bohdanowicz, S. T. Flammia, A. Keller *et al.*, Building a fault-tolerant quantum computer using concatenated cat codes, arXiv:2012.04108 (2020).

[60] V. V. Albert, C. Shu, S. Krastanov, C. Shen, R.-B. Liu, Z.-B. Yang, R. J. Schoelkopf, M. Mirrahimi, M. H. Devoret, and L. Jiang, Holonomic quantum control with continuous variable systems, Phys. Rev. Lett. **116**, 140502 (2016).

[61] R. W. Heeres, P. Reinhold, N. Ofek, L. Frunzio, L. Jiang, M. H. Devoret, R. J. Schoelkopf, Implementing a universal gate set on a logical qubit encoded in an oscillator, Nat. Commun. **8**, 94 (2017).

[62] A. Grimm, N. E. Frattini, S. Puri, S. O. Mundhada, S. Touzard, M. Mirrahimi, S. M. Girvin, S. Shankar, and M. H. Devoret, Stabilization and operation of a Kerr-cat qubit, Nature (London) **584**, 205 (2020).

[63] C. Wang, Y. Y. Gao, P. Reinhold, R. W. Heeres, N. Ofek, K. Chou, C. Axline, M. Reagor, J. Blumoff, K. M. Sliwa et al., A Schrodinger cat living in two boxes, Science **352**, 1087 (2016).

[64] D. Yu, M. M. Valado, C. Hufnagel, L. C. Kwek, L. Amico, and R. Dumke, Charge-qubit-atom hybrid, Phys. Rev. A **93**, 042329 (2016).

[65] O. P. de SaNeto, and M. C. de Oliveira, Quantum bit encoding and information processing with field superposition states in a circuit, J. Phys. B **45**, 185505 (2012).

[66] D. Kim and K. Moon, Hybrid two-qubit gate using circuit QED system with triple-leg stripline resonator, arXiv:1808.02865.

[67] C. P. Yang, Z. F. Zheng, and Y. Zhang, Universal quantum gate with hybrid qubits in circuit quantum electrodynamics, Opt. Lett. **43**, 5765 (2018).

[68] Y. B. Liu, L. Li, and Y. Q. Ma, A Hybrid Rydberg Quantum Gate for Quantum Network, arXiv:2105.00289.

[69] É. Gouzien and N. Sangouard, Factoring 2048-bit RSA Integers in 177 Days with 13 436 Qubits and a Multimode Memory, Phys. Rev. Lett. **127**, 140503 (2021).

[70] M. Sasura, and V. Buzek, Multiparticle entanglement with quantum logic networks: Application to cold trapped ions, Phys. Rev. A **64**, 012305 (2001).

[71] S. L. Braunstein, V. Buzek, and M. Hillery, Quantum network for symmetric and asymmetric cloning in arbitrary dimension and continuous limit, Phys. Rev. A **63**, 052313 (2001).

[72] F. Gaitan, Quantum Error Correction and Fault Tolerant Quantum Computing (CRC Press, USA, 2008).

[73] T. Beth, and M. Rotteler, Quantum algorithms: Applicable algebra and quantum physics, Quantum Information **173**, 96 (2001).

[74] A. Barenco, C. H. Bennett, R. Cleve, D. P. DiVincenzo, N. Margolus, P. Shor, T. Sleator, J. A. Smolin, and H. Weinfurter, Elementary gates for quantum computation, Phys. Rev. A **52**, 3457 (1995).

[75] M. Mötöen, J. J. Vartiainen, V. Bergholm, and M. M. Salomaa, Quantum Circuits for General Multiqubit Gates, Phys. Rev. Lett. **93**, 130502 (2004).

[76] C. P. Yang, Y. X. Liu, and F. Nori, Phase gate of one qubit simultaneously controlling n qubits in a cavity, Phys. Rev. A **81**, 062323 (2010).

[77] M. Waseem, M. Irfan, and S. Qamar, Multiqubit quantum phase gate using four-level superconducting quantum interference devices coupled to superconducting resonator, Physica C **477**, 24 (2012).

[78] H. F. Wang, A. D. Zhu, and S. Zhang, One-step implementation of multiqubit phase gate with one control qubit and multiple target qubits in coupled cavities, Opt. Lett. **39**, 1489 (2014).

[79] C. P. Yang, Q. P. Su, F. Y. Zhang, and S. B. Zheng, Single-step implementation of a multiple-target-qubit controlled phase gate without need of classical pulses, Opt. Lett. **39**, 3312 (2014).

[80] M. Waseem, M. Irfan, and S. Qamar, Realization of quantum gates with multiple control qubits or multiple target qubits in a cavity, Quantum Inf. Process **14**, 1869 (2015).

[81] G. Sun, X. Wen, B. Mao, J. Chen, Y. Yu, P. Wu, and S. Han, Tunable quantum beam splitters for coherent manipulation of a solid-state tripartite qubit system, Nat. Commun. **1**, 51 (2010).

[82] M. Sandberg, C. M. Wilson, F. Persson, T. Bauch, G. Johansson, V. Shumeiko, T. Duty, and P. Delsing, Tuning the field in a microwave resonator faster than the photon lifetime, Appl. Phys. Lett. **92**, 203501 (2008).

[83] Z. L. Wang, Y. P. Zhong, L. J. He, H. Wang, J. M. Martinis, A. N. Cleland, and Q. W. Xie, Quantum state characterization of a fast tunable superconducting resonator, Appl. Phys. Lett. **102**, 163503 (2013).

[84] S. B. Zheng and G. C. Guo, Efficient Scheme for Two-Atom Entanglement and Quantum Information Processing in Cavity QED, Phys. Rev. Lett. **85**, 2392 (2000).

[85] A. Sorensen and K. Molmer, Quantum Computation with Ions in Thermal Motion, Phys. Rev. Lett. **82**, 1971 (1999).

[86] D. F. V. James, and J. Jerke, Effective Hamiltonian theory and its applications in quantum information, Can. J. Phys. **85**, 625 (2007).

[87] E. Schrodinger, Die gegenwaertige situation in der quantenmechanik, Naturwissenschaften **23**, 823 (1935).

[88] M. Silva, and C. R. Myers, Computation with coherent states via teleportations to and from a quantum bus, Phys. Rev. A **78**, 062314 (2008).

[89] L. P. van, Optical hybrid approaches to quantum information, Laser Photonics Rev. **5**, 167 (2011).

[90] U. L. Andersen, J. S. Neergaard-Nielsen, L. P. van, and A. Furusawa, Hybrid quantum information processing, Nat. Phys. **11**, 713 (2015).

[91] D. M. Greenberger, M. A. Horne, and A, Zeilinger, Going beyond Bell's theorem, quantum theory and conceptions of the universe. Springer, Dordrecht, 69-72 (1989).

[92] M. Hillery, V. Buzek, and A. Berthiaume, Quantum secret sharing, Phys. Rev. A **59**, 1829 (1999).

[93] S. Bose, V. Vedral, and P. L. Knight, Multiparticle generalization of entanglement swapping, Phys. Rev. A **57**, 822 (1998).

[94] S. J. Devitt, W. J. Munro, and K. Nemoto, Quantum error correction for beginners, Rep. Prog. Phys. **76**, 076001 (2013).

[95] V. Giovannetti, S. Lloyd, and L. Maccone, Quantum-enhanced measurements: beating the standard quantum limit, Science **306**, 1330 (2004).

[96] J. J. Bollinger, W. M. Itano, D. J. Wineland, and D. J. Heinzen, Optimal frequency measurements with maximally correlated states, Phys. Rev. A **54**, R4649 (1996).

[97] C. P. Yang and S. Y. Han, n-qubit-controlled phase gate with superconducting quantum-interference devices coupled to a resonator, Phys. Rev. A **72**, 032311 (2005).

[98] G. Kirchmair, B. Vlastakis, Z. Leghtas, S. E. Nigg, H. Paik, E. Ginossar, M. Mirrahimi, L. Frunzio, S. M. Girvin, and R. J. Schoelkopf, Observation of quantum state collapse and revival due to the singlephoton Kerr effect, Nature (London) **495**, 205 (2013).

[99] B. Vlastakis, G. Kirchmair, Z. Leghtas, S. E. Nigg, L. Frunzio, S. M. Girvin, M. Mirrahimi, M. H. Devoret, R. J. Schoelkopf, Deterministically encoding quantum information using 100-photon Schrodinger cat states, Science **342**, 607 (2013).

[100] L. Sun, A. Petrenko, Z. Leghtas, B. Vlastakis, G. Kirchmair, K. M. Sliwa, A. Narla, M. Hatridge, S. Shankar, J. Blumoff et al., Tracking photon jumps with repeated quantum non-demolition parity measurements, Nature (London) **511**, 444 (2014).

[101] B. Vlastakis, A. Petrenko, N. Ofek, L. Sun, Z. Leghtas, K. Sliwa, Y. Liu, M. Hatridge, J. Blumoff, L. Frunzio et al., Characterizing entanglement of an artificial atom and a cavity cat state with Bell's inequality, Nat. Commun. **6**, 8970 (2015).

[102] C. P. Yang, Q. P. Su, S. B. Zheng, and S. Han, Generating entanglement between microwave photons and qubits in multiple cavities coupled by a superconducting qutrit, Phys. Rev. A **87**, 022320 (2013).

[103] C. P. Yang and S. Y. Han, Preparation of Greenberger-Horne-Zeilinger entangled states with multiple superconducting quantum-interference device qubits or atoms in cavity QED, Phys. Rev. A **70**, 062323 (2004).

[104] S. L. Zhu, Z. D. Wang, and P. Zanardi, Geometric Quantum Computation and Multiqubit Entanglement with Superconducting Qubits Inside a Cavity, Phys. Rev. Lett. **94**, 100502 (2005).

[105] W. Feng, P. Wang, X. Ding, L. Xu, and X. Q. Li, Generating and stabilizing the Greenberger-Horne-Zeilinger state in circuit QED: Joint measurement, Zeno effect, and feedback, Phys. Rev. A **83**, 042313 (2011).

[106] S. Aldana, Y. D. Wang, and C. Bruder, Greenberger-Horne-Zeilinger generation protocol for N superconducting transmon qubits capacitively coupled to a quantum bus, Phys. Rev. B 84, 134519 (2011).

[107] T. Liu, Q. P. Su, Y. Zhang, Y. L. Fang, and C. P. Yang, Generation of quantum entangled states of multiple groups of qubits distributed in multiple cavities, Phys. Rev. A **101**, 012337 (2020).

[108] I. C. Hoi, C. M. Wilson, G. Johansson, T. Palomaki, B. Peropadre, and P. Delsing, Demonstration of a Single-Photon Router in the Microwave Regime, Phys. Rev. Lett. **107**, 073601 (2011).

[109] J. Koch, T. M. Yu, J. Gambetta, A. A. Houck, D. I. Schuster, J. Majer, A. Blais, M. H. Devoret, S. M. Girvin, and R. J. Schoelkopf, Charge-insensitive qubit design de rived from the Cooper pair box, Phys. Rev. A **76**, 042319 (2007).

[110] M. Baur, A. Fedorov, L. Steffen, S. Filipp, M. P. da Silva, and A. Wallraff, Benchmarking a Quantum Teleportation Protocol in Superconducting Circuits Using Tomography and an Entanglement Witness, Phys. Rev. Lett. **108**, 040502 (2012).

[111] For a transmon qutrit, the $|g\rangle \leftrightarrow |f\rangle$ transition is much weaker than those of the $|g\rangle \leftrightarrow |e\rangle$ and $|e\rangle \leftrightarrow |f\rangle$ transitions. Thus, we have $\gamma_{fg}^{-1} \gg \gamma_{eg}^{-1}, \gamma_{fe}^{-1}$.

[112] C. Rigetti, S. Poletto, J. M. Gambetta, B. L. T. Plourde, J. M. Chow, et al., Superconducting qubit in waveguide cavity with coherence time approaching 0.1 ms, Phys. Rev. B **86**, 100506(R) (2012).

[113] M. J. Peterer, S. J. Bader, X. Jin, F. Yan, A. Kamal, T. J. Gudmundsen, P. J. Leek, T. P. Orlando, W. D. Oliver, and S. Gustavsson, Coherence and decay of higher energy levels of a superconducting transmon qubit, Phys. Rev. Lett. **114**, 010501 (2015).

[114] C. P. Yang, Q. P. Su, and S. Y. Han, Generation of Greenberger-Horne-Zeilinger entangled states of photons in multiple cavities via a superconducting qutrit or an atom through resonant interaction, Phys. Rev. A **86**, 022329 (2012).